Decoherence-protected storage of exciton qubits through ultrafast multipulse control

Thomas E. Hodgson,[1] Lorenza Viola,[2] and Irene D'Amico[1],[*]

[1]*Department of Physics, University of York, Heslington, York YO10 5DD, United Kingdom*
[2]*Department of Physics and Astronomy, 6127 Wilder Laboratory, Dartmouth College, Hanover, New Hampshire 03755, USA*

We quantitatively investigate the usefulness and viability of the scheme developed by Viola and Lloyd [Phys. Rev. A **58**, 2733 (1998)] to control dephasing in the context of exciton-based quantum computation with self-assembled quantum dots. We demonstrate that optical coherence of a confined exciton qubit exposed to phonon-induced dephasing can be substantially enhanced through the application of a simple periodic sequence of control pulses. The shape of the quantum dot has a significant effect on the dephasing properties. Remarkably, we find that quantum dots with parameters optimized for implementing quantum computation are among the most susceptible to dephasing, yet periodic decoupling is most efficient for exactly that type of dot. We also show that the presence of an electric field, which is a necessary ingredient for many exciton-based quantum computing schemes, may further increase the control efficiency. Our results suggest that dynamical decoupling may be a method of choice for robust storage of exciton qubits during idle stages of quantum algorithms.

PACS number(s): 03.67.Lx, 73.21.La, 81.07.Ta

I. INTRODUCTION

The quest for practical implementations of quantum information processing (QIP) (Ref. 1) has resulted in a wide variety of proposed quantum computing architectures based on virtually all kinds of different physical systems.[2] Thanks to continuous advances in nanoscale design and manufacturing of low-dimensional structures, solid-state platforms promise, in particular, a high level of scalability and large-scale integration. Among the various proposals which exist to date, schemes which rely on *charge* degrees of freedom of carriers (*excitons*) confined in a self-assembled semiconductor quantum dot (QD) (Ref. 3) are especially appealing in view of current ultrafast spectroscopic capabilities, which make it possible to access subpicosecond gating times by means of suitable all-optical control techniques.[4,5]

In practice, such advantages are hindered by the rate at which quantum information stored in exciton qubits and/or exciton ancillary states is irreversibly lost due to dephasing—as characterized by a typical time scale T_2. For QD, so-called T_1 processes, which involve energy exchange with the host crystal and lead to finite qubit lifetime via exciton recombination, are highly suppressed due to the large splitting between quantized energy levels. Thus, the dominant contribution to T_2 arises from energy-conserving transitions, which do not change the occupations of the logical states but result in *pure dephasing* and unrecoverable loss of phase information. While typical T_1 times for single QDs are in the nanosecond range, it has been shown theoretically[6–8] and experimentally[9] that substantial dephasing can occur in much shorter time scales (one or two picoseconds at temperatures of a few kelvin) mainly due to coupling with acoustic phonons.

Borrowing inspiration from coherent averaging techniques in high-resolution nuclear-magnetic-resonance spectroscopy,[10] dynamical decoupling (DD) methods have recently emerged in QIP as a versatile strategy for counteracting decoherence from non-Markovian environments in a way which is substantially less resource demanding than traditional quantum error-correcting codes. In its simplest form, DD is implemented by subjecting the system to periodic sequences of fast and strong (so-called *bang bang*) control operations drawn from a basic repertoire so that interactions whose correlation times are long compared to the control time scale are effectively averaged out to finite accuracy.[11,12] In particular, a number of analytical and numerical studies have established the potential for DD schemes based on high-level concatenated[13] or randomized[14,15] design to extend the coherence time of spin degrees of freedom in gate-defined semiconductor QDs by (at least) two orders of magnitude.[16–19] Remarkably, simple DD protocols consisting of a single or multiple spin echoes have been experimentally demonstrated in (gate-defined) double QD devices[20] and rare-earth solid-state centers,[21] respectively.

The usefulness of a suitable burst of ultrashort pulses as a tool to reduce the initial optical dephasing and increasing the final level of polarization in a QD has been demonstrated by Axt *et al.*[22] In this work, we investigate the effectiveness of multipulse DD toward both mitigating the initial coherence decay and ensuring enhanced coherence preservation over a desired storage time scale with emphasis on arbitrary initial states and QIP applications. Our analysis has two main implications: first, we show that in spite of being most prone to dephasing, QDs (which are optimized to support quantum computation) are also most efficiently stabilized by DD. Furthermore, thanks to the fact that the exciton spectral density is down shifted in frequency by the application of a static electric field, DD performance is further improved for a biased QD as required for most computational architectures.[4,23]

The content of this paper is organized as follows. Section II provides an in-depth analysis of the free-dephasing dynamics of an exciton qubit in the absence of applied control. After laying out the relevant QD model in Sec. II A, special emphasis is devoted to isolate and analyze the contributions of the piezoelectric and deformation couplings to the exciton spectral density (Sec. II B) for various dot shapes as well as to quantify the influence of the spectral-density details on the

dephasing behavior. In Sec. III, we summarize our results on the controlled dephasing dynamics and characterize the dependence of DD performance upon different system and control parameters—including dot shape, temperature, separation between pulses, and application of an external bias field. In particular, DD performance for robust exciton storage in QIP applications is highlighted in Sec. III C. Concluding remarks follow in Sec. IV, whereas additional discussion on finite pulse-width effects is included in the Appendix.

II. DEPHASING DYNAMICS OF CONFINED EXCITONS

A. QD model Hamiltonian

We consider a GaAs/AlAs QD with either zero or one ground-state exciton,[8] which corresponds to the qubit logical states $|0\rangle$ or $|1\rangle$, respectively. The Hamiltonian of this two-level excitonic system interacting with the lattice phonon modes may be expressed as

$$H = E_{\text{exc}}c^{\dagger}c + \hbar \sum_{j,\mathbf{k}} \omega_j(\mathbf{k})b_{j,\mathbf{k}}^{\dagger}b_{j,\mathbf{k}} + \hbar c^{\dagger}c \sum_{j,\mathbf{k}} (g_{j,\mathbf{k}}^{*}b_{j,\mathbf{k}}^{\dagger} + \text{H.c.}),$$
$$(1)$$

where E_{exc} is the energy of the ground-state exciton relative to the crystal ground state and $c^{\dagger}(c)$ are creation (annihilation) operators for an exciton. We consider as qubit a ground-state exciton with a well-defined z component of the total angular momentum. This is excited by a resonant circularly polarized laser pulse, e.g., a σ^{+} polarized pulse will couple to the transition between a $(+3/2)$ heavy hole and a $(-1/2)$ conduction electron. $b_{j,\mathbf{k}}^{\dagger}(b_{j,\mathbf{k}})$ are bosonic creation (annihilation) operators for a phonon of mode j, wave vector $\mathbf{k}$, and angular frequency $\omega_j(\mathbf{k})$, and $g_{j,\mathbf{k}}$ is the coupling between an exciton and a phonon of mode $j,\mathbf{k}$, respectively.

We assume that the exciton and the phonon bath are initially uncorrelated with the phonon-bosonic reservoir being in thermal equilibrium at temperature T. As time evolves, the qubit becomes entangled with the environment, and the off-diagonal elements of the exciton density matrix evaluated at time t in the interaction picture with respect to the free system and bath Hamiltonians are given by[6,11]

$$\rho_{01}(t) = \rho_{10}^{*}(t) = \rho_{01}(0)e^{-\Gamma(t)}, \qquad (2)$$

with

$$\Gamma(t) = \int_0^{\infty} d\omega \frac{I(\omega)}{\omega^2} \coth\left(\frac{\hbar\omega}{k_B T}\right)[1 - \cos(\omega t)]. \qquad (3)$$

Here, k_B is the Boltzmann constant, and the spectral function

$$I(\omega) = \sum_{j,\mathbf{k}} \delta(\omega - \omega_j(\mathbf{k}))|g_{j,\mathbf{k}}|^2 \qquad (4)$$

describes the interaction of the qubit with a phonon of frequency $\omega_j(\mathbf{k})$. For an exciton qubit, $\Gamma(t)$ is formally a factor of 4 smaller than for a spin coupled to a bath of harmonic oscillators as described in Ref. 11. This is due to the different Hamiltonians. For the exciton qubit the coupling to the environment only occurs when the qubit is in the logical state $|1\rangle$ (exciton present), while a spin qubit couples to the environment in both logical states.

In order to maximize coherence, we consider sufficiently low temperatures so that the coupling to optical phonons may be safely neglected. For acoustic phonons, we assume the dispersion relation $\omega_j(\mathbf{k}) = v_j|\mathbf{k}|$. In addition, we assume any lattice mismatch at the boundary between the QD and the barrier to be negligible, and therefore, approximate the coupling to the phonon bath as the bulk coupling modulated by the appropriate form factor,[6]

$$g_{j,\mathbf{k}} = \int d^3\mathbf{r}_e d^3\mathbf{r}_h |\Psi(\mathbf{r}_e,\mathbf{r}_h)|^2 (G_{j,\mathbf{k}}^{e}e^{i\mathbf{k}.\mathbf{r}_e} - G_{j,\mathbf{k}}^{h}e^{i\mathbf{k}.\mathbf{r}_h}). \quad (5)$$

Here, $\Psi(\mathbf{r}_e,\mathbf{r}_h)$ is the exciton wave function and $G_{j,\mathbf{k}}^{e/h}$ is the bulk coupling of the single particle to the phonon bath

$$G_{j,\mathbf{k}}^{e/h} = \frac{1}{\sqrt{2\varrho\hbar\omega_j(\mathbf{k})V}}[kD_j^{e/h} + iM_j(\hat{\mathbf{k}})]. \qquad (6)$$

The index j runs over the two transverse and the longitudinal modes, ϱ is the density of the QD, and V is a normalization volume. Excitons in bulk semiconductor couple to longitudinal-acoustic phonons through a deformation-potential coupling $D_j^{e/h}$ and to all the modes considered through a piezoelectric potential coupling M_j. For zinc-blende crystals such as GaAs/AlAs,

$$M_j(\hat{\mathbf{k}}) = \frac{2e_{14}e}{\epsilon_s\epsilon_0}(\hat{k}_x\hat{k}_y\hat{\xi}_z^{(j)} + \hat{k}_y\hat{k}_z\hat{\xi}_x^{(j)} + \hat{k}_z\hat{k}_x\hat{\xi}_y^{(j)}). \qquad (7)$$

In what follows, we shall approximate $|M_j|^2$ by its angular average,[6]

$$\frac{1}{4\pi}\int_0^{2\pi} d\phi \int_0^{\pi} d\theta \sin(\theta)M_j^2(\hat{\mathbf{k}}) = A_j\left(\frac{2ee_{14}}{\epsilon_s\epsilon_0}\right)^2, \qquad (8)$$

where e is the electron charge, e_{14} is the piezoelectric coefficient, and ϵ_s and ϵ_0 denote the relative permittivity of the material and of free space, respectively. $\hat{\xi}_{x/y/z}$ are unit vectors describing the polarization of mode $\mathbf{k}$, and A_j are mode-dependent geometrical factors.

We will consider nanostructures mainly in the strong-confinement regime so that Coulomb coupling may be neglected and excitons may be accurately modeled using products of Gaussian wave packets within the single-particle approximation.[6] We assume that the QD is isotropic in the plane perpendicular to the growth direction. The excitonic wave function is then

$$\Psi(\mathbf{r}_e,\mathbf{r}_h) = \psi(\mathbf{r}_e)\psi(\mathbf{r}_h), \qquad (9)$$

where

$$\psi(\mathbf{r}_{e/h}) = \frac{1}{(\lambda_{r_{e/h}}^2 \lambda_{z_{e/h}} \pi^{3/2})^{1/2}}\exp\left(-\frac{r_{e/h}^2}{2\lambda_{r_{e/h}}^2} - \frac{z_{e/h}^2}{2\lambda_{z_{e/h}}^2}\right), \quad (10)$$

and $2\lambda_{z_{e/h}}$ and $2\lambda_{r_{e/h}}$ are the characteristic widths of the electron/hole wave function in the z (growth) direction and in the plane $r = \sqrt{x^2 + y^2}$, respectively, and are related in the usual way to the characteristic frequencies of the parabolic confining potential in the appropriate direction. For later reference, we define a characteristic volume of the QD,

$$V_\psi \equiv 8\lambda_{r_e}^2 \lambda_{z_e}. \qquad (11)$$

For the exciton-phonon system, Eq. (4) can be written as

$$I_{\text{exc}}(\omega) = I_e(\omega) + I_h(\omega) - 2I_{eh}(\omega), \qquad (12)$$

where $I_{e/h}(\omega)$ is the spectral density of the electron/hole and $I_{eh}(\omega)$ modifies the spectral density due to the electron-hole interference. Each term has the following form:

$$I_s(\omega) \sim \sum_j \omega |G'_{j,s}(\omega)|^2 f_s\left(\frac{\omega \xi_s}{v_j}\right) \exp\left(-\frac{\lambda_{r_s}^2 \omega^2}{2v_j^2}\right), \quad (13)$$

where the index s runs over e, h, and eh,

$$\xi_s^2 = \frac{|\lambda_{z_s}^2 - \lambda_{r_s}^2|}{2}, \qquad (14)$$

and

$$\lambda_{(r/z)_{eh}}^2 = \frac{\lambda_{(r/z)_e}^2 + \lambda_{(r/z)_h}^2}{2}. \qquad (15)$$

The form of $f_s(x)$ depends on the dot shape. For $\lambda_{r_s} > \lambda_{z_s}$ (*oblate*),

$$f_s^{\text{obl}}(x) = \frac{i \, \text{erf}(ix)}{x}, \qquad (16)$$

where $\text{erf}(x)$ is the error function; for $\lambda_{r_s} < \lambda_{z_s}$ (*prolate*),

$$f_s^{\text{pro}}(x) = \frac{\text{erf}(x)}{x}, \qquad (17)$$

and for $\lambda_{r_s} = \lambda_{z_s}$ (*spherical*),

$$f_s^{\text{sph}}(x) = \frac{2}{\sqrt{\pi}}. \qquad (18)$$

In Eq. (13), $|G'_{j,s}(\omega)|^2$ includes terms due to both the deformation potential and the piezoelectric coupling, that is,

$$|G'_{j,s}(\omega)|^2 = \frac{\omega^2}{v_j^2} D_j^{s^2} + |M_j|^2, \qquad (19)$$

where $(D^{eh})^2 = D^e D^h$. This allows the spectral density to be separated into the sum of the spectral densities related to each of the two coupling mechanisms,

$$I_s(\omega) = I_s^{\text{def}}(\omega) + I_s^{\text{piez}}(\omega), \qquad (20)$$

and the total evolution in Eq. (2) to be expressed as a product of contributions from the deformation potential and piezoelectric interactions,

$$e^{-\Gamma(t)} = e^{-\Gamma^{\text{def}}(t)} e^{-\Gamma^{\text{piez}}(t)}. \qquad (21)$$

B. Single particle and excitonic spectral density

The dephasing dynamics of the exciton qubit is determined by the exciton spectral density. In general, $I(\omega)$ is positive, goes to zero as $\omega \to 0$, and becomes negligible for large ω. Aside from the material parameters, the main factor
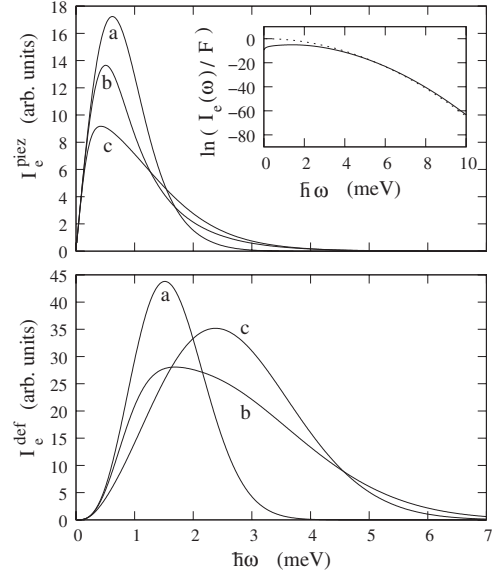

FIG. 1. Piezoelectric $I_e^{\text{piez}}(\omega)$ (top) and deformation $I_e^{\text{def}}(\omega)$ (bottom) contributions to the electron spectral density for the cases of: (a) spherical ($\lambda_{r_e} = 3.84$ nm), (b) oblate ($\lambda_{r_e} = 6$ nm), and (c) prolate QDs ($\lambda_{r_e} = 2$ nm). Inset: $\ln[I_e(\omega)/F]$ for a single electron with $\lambda_{r_e} = 3.84$ nm (solid line). The dashed line is the fitted curve $-2.79 \times 10^{-25} \, \omega^2$ [see Eq. (22)].

influencing the spectral density is the *shape* of the QD,[6] which enters our calculations through the values of $\lambda_{(r/z)_e}$ and $\lambda_{(r/z)_h}$.

To understand the system at hand, we will first consider the behavior of the spectral density for a single trapped particle. Throughout this paper we will consider QDs with $V_{\psi_e} = 455.28$ nm³. For a single particle, for instance an electron, the maximum of the spectral density is greatest for a spherical QD. For oblate or prolate QDs with the same characteristic volume V_ψ, the spectral density has a lower maximum but extends to higher frequencies. The top panel of Fig. 1 shows the piezoelectric spectral densities for a single electron, I_e^{piez}, for different dot shapes. As the dot becomes more asymmetric, the interplay between $f_e(\omega \xi_e/v_j)$ and the Gaussian term in Eq. (13) reduces the maximum of $I_e^{\text{piez}}(\omega)$ while increasing $I_e^{\text{piez}}(\omega)$ at high frequencies.

For the deformation-potential coupling, the single-particle spectral densities follow a similar trend, however, the extra ω^2 term in the expression for $I_e^{\text{def}}(\omega)$ [see Eq. (19)] results in larger $I_e^{\text{def}}(\omega)$ at high frequencies. The bottom panel of Fig. 1 shows the deformation-potential spectral densities for a single electron in QDs with different shapes. We can define an effective upper cut-off frequency ω_c such that $I(\omega)$ is negligible for $\omega \gg \omega_c$. The QD spectral density is composed of a sum of terms each containing a Gaussian function. The high-frequency behavior of the overall function is therefore very similar to a Gaussian, thus, we may write

$$I(\omega) \approx F e^{-\omega^2/\omega_c^2}, \quad F > 0, \qquad (22)$$

and treat ω_c as the cut-off frequency. In order to obtain a value for ω_c, we fit this form to our numerical results. The inset of Fig. 1 shows $\ln[I(\omega)/F]$ for a single electron in a

TABLE I. Material parameters for GaAs QDs from Ref. 8. m_0 denotes the free-electron mass.

Static dielectric constant	ϵ_s	12.53
Longitudinal sound velocity (m/s)	v_L	5110
Transverse sound velocity (m/s)	v_T	3340
Density (g/cm^3)	ϱ	5.37
Electron deformation potential (eV)	D_e	7.0
Hole deformation potential (eV)	D_h	-3.5
Piezoelectric constant (C/m^2)	e_{14}	0.16
Effective electron mass (m_0)	m_e	0.067
Effective hole mass (m_0)	m_h	0.34
Longitudinal geometrical factor	A_L	3/35
Transverse geometrical factor	A_T	1/21

spherical QD ($\lambda_{r_e} = 3.84$ nm) along with fitted curve with parameters $F = 7.9 \times 10^{12}$ s^{-2} and $\omega_c = 1.89 \times 10^{12}$ rads^{-1} ($\hbar\omega_c = 1.25$ meV).

For an exciton in a self-assembled QD, the electron and hole confinements in the z (growth) direction are due to the band offset between the barrier and dot layers. Therefore the electron and hole widths are determined by the thickness of these layers and $\lambda_{z_e} \approx \lambda_{z_h}$. The radial in-plane confinement, however, may be different for electron and hole and is accurately modeled by harmonic potentials. This leads to

$$\lambda_{r_h} = \sqrt{\frac{m_e^* \omega_e}{m_h^* \omega_h}} \lambda_{r_e}, \tag{23}$$

where $\omega_{e/h}$ is the characteristic frequency of the confining potential for the electron/hole and $m_{e/h}^*$ is the electron/hole effective mass. Throughout this paper, we shall discuss GaAs QDs,[23] the material parameters of which are listed in Table I. Because of Eq. (23), the electron and hole wave functions are not simultaneously spherical for a given QD. There are three possible regimes for the exciton wave function. For a heavily prolate QD, both the electron and hole wave functions are prolate (*prolate-prolate regime*), similarly for heavily oblate QDs, the wave functions are both oblate (*oblate-oblate regime*). In between these two situations, the electron and hole will stretch in different directions (*oblate-prolate regime*). The most symmetric configuration in the oblate-prolate regime occurs when $\xi_e = \xi_h$, corresponding to the following radial confinement:

$$\bar{\lambda}_{r_e} = \left[\frac{V_\psi^e}{\sqrt{32}[1 + (m_e^* \omega_e / m_h^* \omega_h)]} \right]^{1/3}. \tag{24}$$

In the results plotted throughout the paper, we shall assume $\hbar\omega_e / \hbar\omega_h = 1.25$, which corresponds to the parameters for the optimal dot for quantum computation discussed in Ref. 23.

For the excitonic system, there is an additional difference between the form of the spectral-density components due to piezoelectric and deformation-potential couplings: for piezoelectric coupling, the interference term I_{eh}^{piez} is always positive, whereas for deformation-potential interaction both signs are possible depending on material properties. For GaAs, I_{eh}^{def}
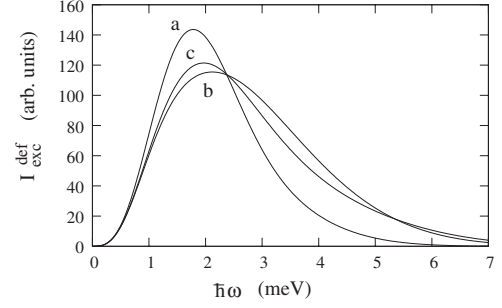

FIG. 2. Excitonic deformation spectral density $I_{\text{exc}}^{\text{def}}(\omega)$ for the cases of: (a) $\lambda_{r_e} = \bar{\lambda}_{r_e} = 4.16$ nm, (b) oblate-oblate regime ($\lambda_{r_e} = 6$ nm), and (c) prolate-prolate regime ($\lambda_{r_e} = 3$ nm).

is negative and is of the same order of I_e^{def} and I_h^{def}. As a consequence, $I_{\text{exc}}^{\text{def}}$ behaves similarly to the single-particle spectral density, in that it has a lower maximum in the prolate-prolate and oblate-oblate regimes compared to QDs with $\lambda_{r_e} \approx \bar{\lambda}_{r_e}$, but $I_{\text{exc}}^{\text{def}}$ will be greater for large ω.

Figure 2 shows the deformation-potential spectral density $I_{\text{exc}}^{\text{def}}$ for different dot shapes. Notice that at $\lambda_{r_e} = \bar{\lambda}_{r_e}$, the electron wave function is as oblate as the hole wave function is prolate; for deformation-potential coupling, $I_{\text{exc}}^{\text{def}}$ behaves similarly for $\lambda_{r_e} > \bar{\lambda}_{r_e}$ as for $\lambda_{r_e} < \bar{\lambda}_{r_e}$.

For piezoelectric coupling, the different sign of the interference term I_{eh}^{piez} leads to a very different behavior of the spectral density. First, if the electron and hole wave functions were exactly the same, there would be no piezoelectric coupling, that is, $I_{\text{exc}}^{\text{piez}} = 0$. At low frequencies, $I_e^{\text{piez}}(\omega) \approx I_h^{\text{piez}}(\omega)$, and their sum cancels with the contribution from the interference term leading to $I_{\text{exc}}^{\text{piez}} \sim 0$. The width of this depletion of the spectral density is greater for smaller λ_{r_e}. For dots in the oblate-oblate regime ($\lambda_{r_e} > 4.85$ nm), as λ_{r_e} is decreased the maximum of the piezoelectric exciton spectral density increases, however, it also shifts toward higher-frequency modes as shown in the top panel of Fig. 3. As λ_{r_e} decreases further, we first enter the oblate-prolate regime (3.84 nm $< \lambda_{r_e} < 4.85$ nm) and then the prolate-prolate regime ($\lambda_{r_e} < 3.84$ nm). As λ_{r_e} reduces to even smaller values, the piezoelectric spectral density becomes small for all ω. This is due to the type of confinement in the growth direction, which results in $\lambda_{z_e} = \lambda_{z_h}$. In this limit, $\xi_e \approx \xi_h$ and $I_e^{\text{piez}} + I_h^{\text{piez}} - 2I_{eh}^{\text{piez}} \approx 0$ for all ω. This behavior may be seen in the bottom panel of Fig. 3, in which $I_{\text{exc}}^{\text{piez}}$ is plotted for values of decreasing λ_{r_e}. We shall denote the value of λ_{r_e}, which yields the largest maximum of $I_{\text{exc}}^{\text{piez}}$, as $\bar{\lambda}_{r_e}^{\text{piez}}$ with $\bar{\lambda}_{r_e}^{\text{piez}} \gtrsim \bar{\lambda}_{r_e}$. For $V_{\psi_e} = 455.28$ nm^3, $\bar{\lambda}_{r_e}^{\text{piez}} = 5.58$ nm. The discrepancy between $\bar{\lambda}_{r_e}$ and $\bar{\lambda}_{r_e}^{\text{piez}}$ is due to the constraint $\lambda_{z_e} = \lambda_{z_h}$. Again, we may follow the same method as in the single-electron case to define and estimate a spectral cutoff ω_c. For an exciton with $\lambda_{r_e} = \bar{\lambda}_{r_e} = 4.16$ nm, this yields $\omega_c = 3.52 \times 10^{12}$ rads^{-1} ($\hbar\omega_c = 2.32$ meV), i.e., ω_c is of the same order as the single-particle case for a spherical QD.

C. Effect of spectral density on exciton dephasing

Insight into the dephasing properties may be obtained by examining the evolution of the off-diagonal density-
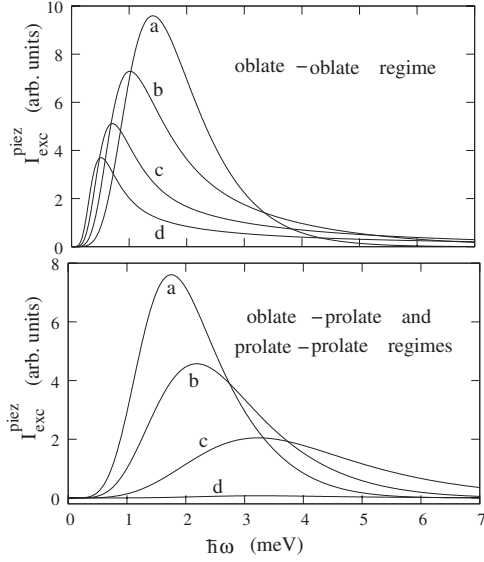
FIG. 3. Top panel: Excitonic piezoelectric spectral density $I_{exc}^{piez}(\omega)$ in the oblate-oblate regime for the cases of increasing λ_{r_e}: (a) $\lambda_{r_e}=6$, (b) 9, (c) 13, and (d) 18 nm. Bottom panel: $I_{exc}^{piez}(\omega)$ in the oblate-prolate and prolate-prolate regimes, respectively, for decreasing λ_{r_e}. (a) $\lambda_{r_e}=4$, (b) 3, (c) 2, and (d) 1 nm.

matrix elements with time [Eq. (2)]. Physically, the coherence element $\rho_{01}(t)$ is proportional to the system optical polarization $\mathbf{P}(t)$ [see, e.g., Eq. (9) in Ref. 6]. In order to emphasize this relation, we have chosen to monitor the quantity $|e^{-\Gamma(t)}|^2=|\mathbf{P}(t)|^2/|\mathbf{P}(t=0)|^2$. Figure 4 shows the decoherence factor $|\exp[-\Gamma(t)]|^2$ for $\lambda_{r_e}=6.16$ nm at 4 K. $|\exp[-\Gamma(t)]|^2$ falls quickly from unity before saturating at temperature- and shape-dependent values. For the examples in Fig. 4, the asymptotic coherence is appreciably larger than zero, however, at higher temperatures and for differently shaped dots, ρ_{01} may be vanishingly small.[6]
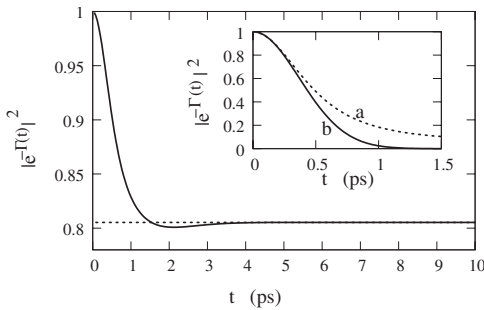

FIG. 4. Decoherence dynamics for $\lambda_{r_e}=6.16$ nm at 4 K (solid line) and asymptotic decoherence value from Eq. (25) (dashed line). Inset: Decoherence dynamics for $\lambda_{r_e}=6.16$ nm at 77 K using: (a) exact results and (b) the short-time approximation from Eq. (26).
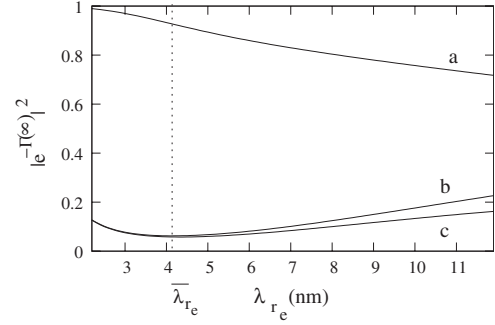

FIG. 5. Asymptotic decoherence factor $|\exp[-\Gamma(\infty)]|^2$ versus λ_{r_e} for: (a) deformation-potential coupling, (b) piezoelectric coupling, and (c) both effects included for an exciton at $T=77$ K.

More specifically, in the limit of $t\rightarrow\infty$, Eq. (3) becomes

$$\Gamma(\infty) = \int_0^\infty d\omega \frac{I(\omega)}{\omega^2}\coth\left(\frac{\hbar\omega}{k_BT}\right), \qquad (25)$$

therefore, the nondiagonal density matrix may saturate to a finite value if $I(\omega) \overset{\omega\rightarrow 0}{\sim} \omega^3$. This was discussed for specific spectral-density functions in Refs. 6 and 24. Saturation at a nonzero value does not occur for the (free) spin-boson system with Ohmic spectral density analyzed in Ref. 11. Figure 5 shows the asymptotic coherence value $|\exp[-\Gamma(\infty)]|^2$ as a function of λ_{r_e} for an exciton at 77 K in the presence of (i) deformation-potential coupling alone, (ii) piezoelectric coupling alone, and (iii) both effects included. For the piezoelectric interaction, $\Gamma^{piez}(\infty)\rightarrow 0$ as $\lambda_{r_e}\rightarrow 0$ due to the fact that $I_{exc}^{piez}\rightarrow 0$ (Fig. 3). As λ_{r_e} increases, $\Gamma^{piez}(\infty)$ becomes large, reflecting the fact that the asymmetry between electron and hole wave functions becomes relevant therefore increasing the piezoelectric coupling. For the deformation-potential coupling, $\Gamma^{def}(\infty)$ is maximum (very close to $\bar{\lambda}_{r_e}$). The results in Fig. 5 are calculated at a temperature of 77 K. The magnitude of the dephasing can be reduced by considering lower temperatures.

Let us now consider the opposite-time limit. The short-time decoherence behavior offers insight into how the spectral density affects the initial dephasing rate, that is, how fast $\exp[-\Gamma(t)]$ falls from unity. For small t, Eq. (3) becomes

$$\Gamma(t) \approx \frac{t^2}{2}\int_0^\infty d\omega I(\omega)\coth\left(\frac{\hbar\omega}{k_BT}\right). \qquad (26)$$

Equation (26) shows that at short times $\exp[-\Gamma(t)]$ has a Gaussian shape with a width that depends on the structure and material parameters as well as temperature. The inset of Fig. 4 compares the approximation of Eq. (26) with the exact dephasing curve [Eq. (3)].

For the piezoelectric interaction, the rate at which $|\exp[-\Gamma^{piez}(t)]|^2$ falls from unity is temperature dependent but for low temperatures the fastest dephasing [that is, the minimum width of the Gaussian in Eq. (26)] occurs for $\lambda_{r_e}\approx\bar{\lambda}_{r_e}^{piez}$: At 4 K, for instance, the fastest dephasing happens at $\lambda_{r_e}\approx 6.18$ nm. For more oblate/prolate QDs, the initial

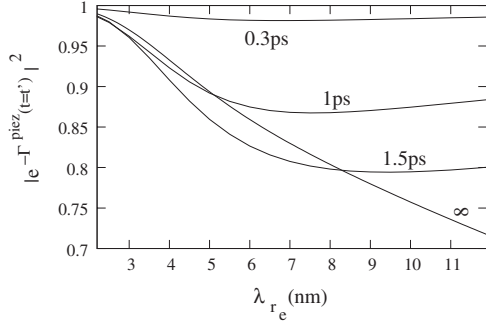FIG. 6. Dependence of fixed-time dephasing due to piezoelectric coupling, $|\exp[-\Gamma^{\mathrm{piez}}(t=t')]|^2$, with respect to λ_{r_e} for an exciton at 77 K. (a) $t'=0.3$, (b) 1, and (c) 1.5 ps. In (d), the long-time decay $|\exp[-\Gamma^{\mathrm{piez}}(\infty)]|^2$ is also depicted.

dephasing occurs slower. Figure 6 shows $|\exp[-\Gamma^{\mathrm{piez}}(t=t')]|^2$ evaluated at different evolution times as a function of λ_{r_e} and at $T=77$ K. The short-time dephasing ($t' \lesssim 0.3$ ps) becomes negligible for small λ_{r_e} as $I^{\mathrm{piez}} \to 0$. Depending on λ_{r_e}, dephasing may not be monotonic with time. For example, in Fig. 6, $|\exp[-\Gamma^{\mathrm{piez}}(1.5\ \mathrm{ps})]|^2 < |\exp[-\Gamma^{\mathrm{piez}}(\infty)]|^2$ for $\lambda_{r_e} \lesssim 8$ nm. This is due to the existence of a local minimum in the evolution of $|\exp[-\Gamma^{\mathrm{piez}}(t)]|^2$ before saturation occurs[6] (see Fig. 4).

For deformation-potential coupling, the width of the Gaussian in Eq. (26) is locally maximum for QDs with λ_{r_e} close to $\bar{\lambda}_{r_e}$. At 4 K, this occurs at $\lambda_{r_e} \approx 4.3$ nm. The short-time dephasing becomes negligible for very large and very small λ_{r_e} (see Fig. 7, where $t=0.3$ ps). For low temperatures, a local minimum of the dephasing occurs near $\bar{\lambda}_{r_e}$. As the temperature is increased, the local minimum is flattened and becomes a global maximum (see Fig. 7).

III. PERIODICALLY CONTROLLED EXCITON DEPHASING DYNAMICS

Having clarified the essential features of the phonon-induced dephasing dynamics in the absence of control, we now show how it can be substantially reduced through DD. Our main goal here is to assess the benefits resulting from
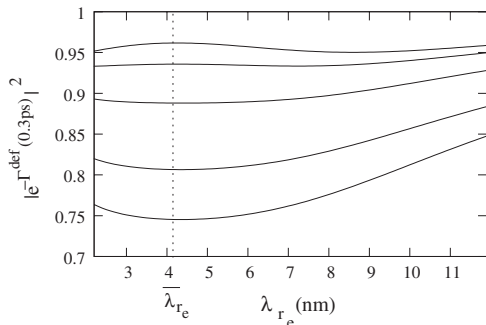

FIG. 7. Dependence of short-time dephasing due to deformation coupling, $|\exp[-\Gamma^{\mathrm{def}}(t=0.3\ \mathrm{ps})]|^2$, upon λ_{r_e} for an exciton at different temperatures: (a) 4, (b) 15, (c) 30, (d) 56, and (e) 77 K.

the application of DD in its simplest periodic form involving repeated bit flips as in Ref. 11.

A. Control setting

We implement dynamical decoupling (DD) by subjecting the exciton to a train of uniformly spaced ideal π pulses applied at instants $t_\ell = \ell \Delta t$, where $\ell = 1, 2, \ldots$ with $\Delta t > 0$ being the separation between consecutive pulses. $T_c = 2\Delta t$ defines a complete DD cycle, which brings the control propagator back to unity. Under resonance conditions, the controlled dephasing dynamics in the presence of a rotating field may be described by a modified decoherence function,[11]

$$\Gamma(t) = \int_0^\infty d\omega \frac{I(\omega)}{\omega^2} \coth\left(\frac{\hbar\omega}{k_B T}\right)[1 - \cos(\omega t)]\tan^2\left(\frac{\omega \Delta t}{2}\right),$$

(27)

where time is understood to be stroboscopically sampled at integer multiples of the control cycle time $t = NT_c = 2N\Delta t$.

In practice, the required control rotations may be effected through suitable laser pulses. On resonance, the exciton qubit will Rabi oscillate between the logical states, and a pulse of appropriate length will perform a bit flip. Equation (27) assumes that such bit flips are instantaneous, which is an adequate approximation provided that the time necessary to perform each bit-flip operation is much shorter than any other time scale relevant to the problem. In order to consistently model the evolution of excitonic qubits, a constraint must be placed on the timing of the control pulses. The central energy of a control pulse must be resonant with the energy of the ground-state exciton, and its frequency spread must be small enough such that the probability of exciting higher-energy levels is negligible. This places a lower bound on the pulse length, as too short a pulse would excite higher-energy levels of the quantum dot (QD), and in extreme circumstances ionize the electron. To account for this (in a model which assumes instantaneous bit flips), the delay between bit flips must be significantly longer than the minimum length of each control pulse.

The relevant energy scale in this case is the difference between the ground-state and higher-energy levels, and in the strong-confinement regime of interest here, this can be of the order of tens of meV. This translates into a minimum pulse length of the order of a few tens of femtoseconds and a constraint on the interval between control pulses of the order of a few tenths of a picosecond. Quantitative evidence justifying this approximation is included in the Appendix. Finally, we assume that the lattice relaxation time is much greater than the interval between pulses and that no systematic and/or random control errors affect the DD operations.

B. Dephasing suppression through multipulse control

Figure 8 shows the decoherence factor, $|\exp[-\Gamma(t)]|^2$, for $\lambda_{r_e} = 6.16$ nm at 77 K in the presence of a DD sequence with different pulse delays, whereas the inset compares the free evolution with the controlled evolution on a smaller time scale for the case of $\Delta t = 0.25$ ps. Decreasing the pulse sepa-
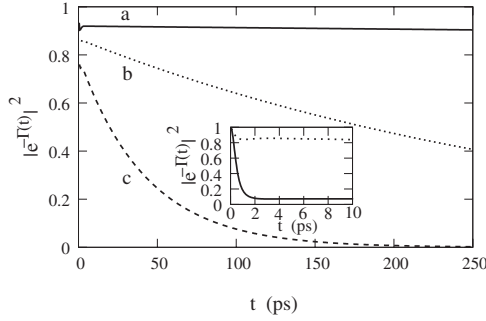
FIG. 8. Decoherence dynamics, $|\exp[-\Gamma(t)]|^2$, for λ_{r_e} =6.16 nm at 77 K under periodic DD with: (a) Δt=0.2, (b) 0.25, and (c) 0.3 ps. Inset: Free (solid line) and controlled (dotted line) evolutions for the case of Δt=0.25 ps.

ration Δt decreases the dephasing for two reasons: first, the qubit dephases slower in the presence of more closely separated control pulses, and second the control sequence begins at an earlier instant, thus, less coherence is lost before the first control pulse occurs.

As expected, the dephasing follows the free evolution until the first bit flip occurs, after which a transient regime sets in during the first few control cycles. Eventually, the controlled coherence decays away to zero but over a substantially longer time scale than the one associated with the free evolution. Our numerical results suggest that no saturation at a nonzero value takes place for the controlled evolution in the relevant parameter regime, however, the coherence decay time increases with decreasing Δt. This is apparent when comparing the controlled evolution over different time scales, e.g., compare the dotted lines in the main panel and the inset of Fig. 8, respectively, which show the evolution for Δt=0.25 ps. As long as DD is turned on early enough, there exists a time interval in which the controlled evolution dephases less than the free evolution. This time interval can be orders of magnitude greater than the free-evolution dephasing and excitonic recombination times.

Beside depending on the control time scale Δt, the DD efficiency is influenced by the shape of the dot, which enters Eq. (27) through the spectral density $I(\omega)$ analyzed in Sec. II C. Alternatively, one may regard the controlled decoherence behavior as being determined by a DD-renormalized spectral density $I(\omega)\tan^2(\omega\Delta t/2)$. The last term presents a resonance at $\omega_{\text{res}}=\pi/\Delta t$, which is the characteristic frequency introduced by the periodic pulsing. The smaller Δt, the higher this characteristic frequency is. Although the time-dependent contribution prevents the integrand from diverging to infinity, the location of ω_{res} relative to the bare spectral density plays a crucial role in determining the dephasing properties: at sufficiently long time t, the largest contribution to $\Gamma(t)$ for our system originates from frequencies close to ω_{res}. Therefore, DD is expected to be efficient provided that $\omega_{\text{res}} \gtrsim \omega_c$, i.e., physically, the control cycle time T_c becomes significantly smaller than the correlation time scale τ_c $=2\pi/\omega_c$.[25]

For control separations Δt=0.3 ps, ω_{res}=1.04 $\times 10^{13}$ rads^{-1} ($\hbar\omega_{\text{res}}$=6.85 meV), which corresponds to frequencies $\omega \gtrsim \omega_c$ such that $I_{\text{exc}}(\omega)$ may become negligible
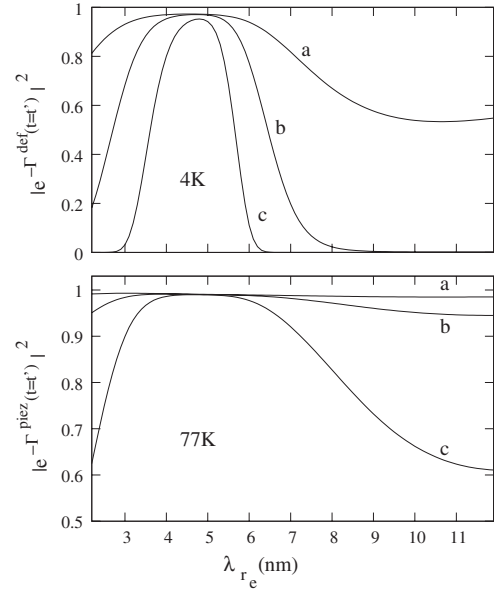

FIG. 9. Deformation decoherence factor $|\exp[-\Gamma^{\text{def}}(t')]|^2$ for an exciton at 4 K (top panel) and piezoelectric decoherence factor $|\exp[-\Gamma^{\text{piez}}(t')]|^2$ for an exciton at 77 K (bottom panel) as a function of λ_{r_e} in the presence of a sequence of DD pulses separated by Δt=0.3 ps for different evolution times: (a) t'=3, (b) 30, and (c) 300 ps.

depending on the shape of the dot (see Figs. 2 and 3). In particular, the optimally shaped QD for DD is the one with the smallest $I_{\text{exc}}(\omega_{\text{res}})$. For V_{ψ_e}=455.28 nm^3 and Δt=0.3 ps, this yields λ_{r_e}=4.8 nm. The top panel of Fig. 9 depicts the decoherence factor due to deformation coupling, $|\exp[-\Gamma^{\text{def}}(t')]|^2$, for an exciton at 4 K subject to a DD sequence with Δt=0.3 ps evaluated at various evolution times t'. Full dephasing may occur for very oblate/prolate QDs, however, there is also a local maximum in the efficiency of the control sequence, which for large t' occurs for dots with λ_{r_e}=4.8 nm. This is due to this particular shape of dot having the smallest $I_{\text{exc}}^{\text{def}}(\omega_{\text{res}})$. The bottom panel of Fig. 9 shows the piezoelectric contribution, $|\exp[-\Gamma^{\text{piez}}(t')]|^2$, for an exciton at 77 K in the same control settings. Once again, the local maximum in the DD efficiency for large t' is determined by λ_{r_e}, which minimizes $I_{\text{exc}}^{\text{piez}}(\omega_{\text{res}})$. At lower temperatures, the overall magnitude of the dephasing is reduced.

The separate components of the spectral density, I_e, I_h, and $-2I_{eh}$ for a QD with λ_{r_e}=4.8 nm (corresponding to the minimum dephasing in the top panel of Fig. 9), are plotted in Fig. 10. The components of the spectral density include contributions from both piezoelectric and deformation-potential couplings. For this reason, the interference term I_{eh} includes both negative and positive terms. It can be seen that I_{exc} $\approx I_h$ for $\hbar\omega \gtrsim 5$ meV. Therefore, close to the local minimum of the dephasing, we can identify the dot shape needed to minimize the dephasing by choosing λ_{r_e} such that I_h is minimized at high ω. This occurs when the hole wave function is spherical. For V_{ψ_e}=455.28 nm^3 and GaAs (i.e., λ_{r_h} =0.495λ_{r_e}), this corresponds to λ_{r_e}=4.856 nm, which is consistent with the minimum dephasing value of λ_{r_e}=4.8 nm. The small difference is due to the contributions to $I_{\text{exc}}(\omega_{\text{res}})$ from I_{eh} and I_e (see inset of Fig. 10).
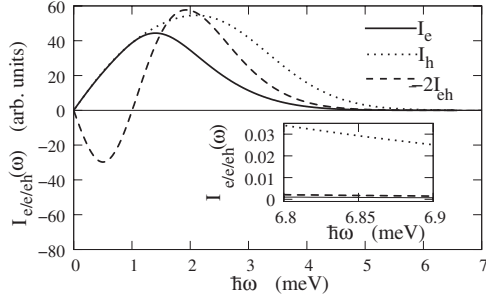
FIG. 10. Spectral-density contributions $I_e(\omega)$, $I_h(\omega)$, and $-2I_{eh}(\omega)$ for a QD with λ_{r_e}=4.8 nm. Inset: $I_e(\omega)$, $I_h(\omega)$, and $-2I_{eh}(\omega)$ at $\omega=\omega_{\mathrm{res}}=10.4\times10^{-12}$ rads^{-1}.

Note that, as the limit of very fast control is approached ($T_c \ll \tau_c$), the shape of the dot has a smaller influence on the exciton coherence, which generally remains close to its value at the instant the first pulse occurred for a long period of time.

C. DD performance for exciton qubits

Let us now specifically focus on QDs intended for quantum computation applications.[23] We will consider two sets of parameters, QDs A and B. QD A is a GaAs QD with an AlAs barrier. The confining potentials are modeled as parabolic in all three dimensions with electron (hole) confinement energies in the z direction of $\hbar\omega_e$=505 meV ($\hbar\omega_h$=100 meV) and $\hbar\omega_e$=30 meV ($\hbar\omega_h$=24 meV) in the in-plane directions, respectively. This corresponds to λ_{r_e}=6.16 nm, λ_{r_h} =3.05 nm, and $\lambda_{z_e}=\lambda_{z_h}$=1.5 nm. QD B is the same dot, except an external electric field of 75 kV/cm is applied in the x direction. QD B has been shown to be suitable for quantum information-processing schemes, which exploit direct Coulomb coupling between excitons,[23] whereas QD A may be useful in schemes not based on the biexcitonic shift. The time evolution of the off-diagonal density-matrix elements for the free-dephasing dynamics [Eq. (2)] for QDs A and B is depicted in Fig. 11 for different temperatures.[8,26]

Figure 12 shows the qubit coherence evolution for both QDs in the presence of periodic DD according to Eq. (3). The left column corresponds to QD A and the right to QD B. Temperatures are 4, 77, and 300 K from top to bottom. It can be seen that for pulses separated by $\Delta t \lesssim 0.2$ ps, DD approximately freezes the dephasing over the time scales relevant to the problem. For a control sequence with longer pulse delays, the qubit coherence decays more rapidly, however, dephasing can still be strongly suppressed for relatively long times.

In terms of practical quantum computation, the bit flips do not change the time taken for the onset of decoherence, that is, the initial time taken for $e^{-\Gamma(t)}$ to sharply decrease from unity. The qubit follows its free evolution until the first bit flip occurs, which (due to the physical constraint on Δt) happens after some coherence is lost. Still, the pulse sequence succeeds at significantly enhancing the exciton coherence at large t. For certain operating temperatures and/or QD devices, the resulting coherence level may remain very close to
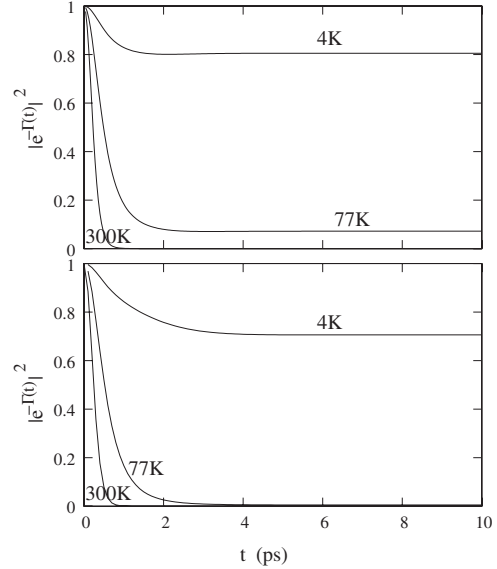
unity, e.g., for QD B at 4 K and Δt=0.1 ps, $\rho_{01}(t=10 \text{ ps})$ = $\sqrt{0.997}\rho_{01}(t=0)$, to be contrasted with the free-evolution value of $\sqrt{0.706}\rho_{01}(t=0)$ (see right upper panel). Even at room temperature, where for the free evolution all coherence

FIG. 11. Free-dephasing dynamics of QDs A (upper panel) and B (lower panel) for different temperatures.
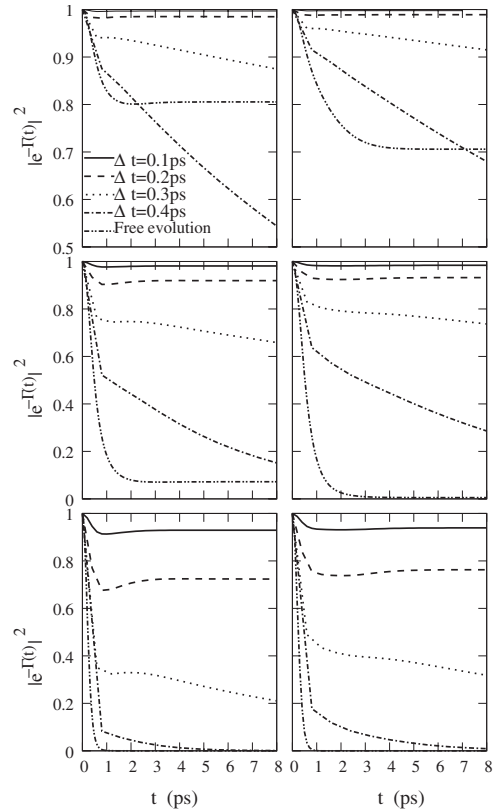

FIG. 12. Controlled dephasing dynamics of QDs A (left) and B (right) at 4 (top), 77 (middle), and 300 K (bottom) for different pulse separations.
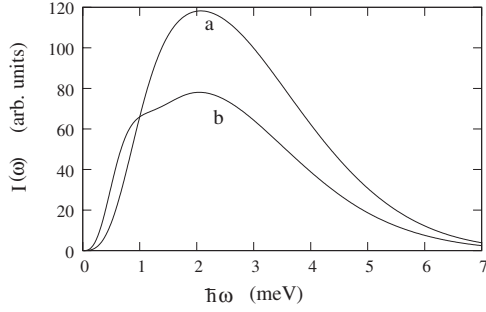
FIG. 13. Spectral density $I(\omega)$ for (a) exciton in QD A and (b) exciton in QD B.

is lost in the first picosecond, our calculations show that for $\Delta t = 0.1$ ps, $\rho_{01}(t) > \sqrt{0.929}\rho_{01}(t=0)$ for both QDs A and B for a long period of time.

It is important to note that in the presence of DD, the qubit subject to the applied electric field (QD B) dephases *less* than without applied field (compare left and right columns of Fig. 12). This is in contrast to the free-evolution behavior, whereby the presence of an electric field increases the coupling to the piezoelectric field and enhances the dephasing. However, a static electric field increases the coupling between excitonic qubits and significantly improves the feasibility of quantum computation. Our results demonstrate that an electric field actually *increases* the efficiency of periodic DD.

This improvement may be understood by looking at the exciton spectral density. Figure 13 compares the spectral density for the exciton with and without electric field. It can be seen that the spectral density in the presence of an electric field is shifted to *lower* frequencies compared to the no-field case. This leads to larger long-term dephasing [see Eq. (25)], in a way, similar to the increase in dephasing due to the piezoelectric field as λ_{r_e} increases. Introducing the electric field effectively causes the piezoelectric coupling to contribute more significantly to the dephasing than the deformation-potential coupling[8] due to the nonvanishing electron-hole dipole moment. Because the relevant spectral density is proportional to the Fourier transform of the wave function, the relative shift of the electron and hole wave functions results in a narrower spectral density. In particular, it decreases the spectral density at high frequencies (see Fig. 13). As a result, the efficiency of sufficiently fast DD sequences ($\omega_c \Delta t \lesssim \pi$) is increased due to a lower contribution at ω_{res} as discussed in Sec. III B. More generally, any phenomenon which decreases the spectral density at ω_{res} will automatically improve DD performance.

Also note that for very short pulse separations ($\omega_c \Delta t \ll \pi$), coherence is maintained near its value at the instant of the first control pulse. Since the applied electric field leads to a slower initial dephasing than the no-field case, less coherence has been lost at the instant of the first control pulse, thus, ρ_{01} remains at a higher value. Again, this is similar to the piezoelectric dephasing behavior observed for increasing λ_{r_e}.

The presence of an electric field, or a QD shape, such that λ_{r_e} is close to $\bar{\lambda}_{r_e}$, $\bar{\lambda}_{r_e}^{\mathrm{piez}}$ leads to greater free dephasing both in

terms of the speed of the initial dephasing as well as the magnitude at which coherence saturates as seen in Sec. II C. However, our results show that it is precisely for these QDs that the DD scheme is most efficient for the shortest control sequences allowed by the physical system. Specifically, the QDs described in this section have $\lambda_{r_e} = 6.16$ nm, which is close to that for which DD is most efficient (see Fig. 9). Slightly changing the dot dimensions so that λ_{r_e} becomes closer to the ideal value would further improve the results reported in Fig. 12.

IV. DISCUSSION AND CONCLUSIONS

We have shown that the dephasing of an exciton qubit due to its coupling with the lattice phonons can be significantly decreased by coherent dynamical control. We found that while quantum dots with a size and shape most suitable for quantum computation are the most prone to dephasing, periodic dynamical decoupling is most efficient for exactly this type of dot. We have demonstrated that a good estimate for the shape of the dot, which optimizes decoupling performance, is the one where the *hole wave function is spherical*. In addition, our analysis indicates that, although the presence of an electric field (which is required by most exciton-based quantum computing schemes) increases dephasing, it also makes for improved decoupling performance. In the presence of periodic decoupling, the decay of qubit coherence is substantially reduced for evolution times, which are very long compared to typical gating times. Under favorable circumstances, it is reduced so significantly that in practical terms, the qubit no longer dephases.

Experiments have shown that often the ground-state excitonic transition in self-assembled quantum dots presents a fine structure, which admixes the excitons with different angular momentum. Ref. 27 demonstrated though that this exchange splitting between excitons can be "switched off" by doping the dot with an additional charge. For the strongly confined structures we are interested in, it is known[28] that the effect of this type of doping is simply to cause a shift in the energy levels with a negligible effect on the excitonic wave-function shape, which governs the coupling between phonons and excitons. We can envision using such a doping strategy in order to overcome potential problems due to the excitonic fine structure.

From an implementation perspective, the main significance of our results lies in their potential for a dephasing-protected exciton quantum memory. In standard solid-state quantum computation schemes, holes in double dots[29] and spin qubits[28] are employed for long-term quantum information storage due to longer T_1 lifetimes, while exciton qubits are usually proposed for computation only, often as ancillary states, and used for gating purposes. Still, quantum algorithms are generally built up of a series of gates, and *arbitrary* qubit states may have to be stored on demand while other gate operations are carried out. We propose that dynamical decoupling in the simplest periodic implementation examined here be invoked to achieve *robust temporary data storage* during the idle stages of computation.

Beside assessing the impact of pulse imperfections, which are unavoidably present in real control systems, several ex-

tensions of the present analysis may be worth considering in order to both further boost quantum storage fidelities and, more ambitiously, to achieve dynamically corrected quantum processing. In particular, dynamical decoupling schemes, which involve nonuniform time delays and are based on either recursive concatenated design[13] or direct cancellation of high-order error terms,[30] have been recently found to attain remarkable high decoupling fidelity under appropriate assumptions.[13,17,31] Furthermore, so-called Eulerian decoupling schemes[32] allow decoherence suppression to be achieved while minimizing the required control amplitude—which may be useful to further minimize unwanted excitations. A future investigation will be needed to identify the possible added benefits of more elaborated decoupling schemes under the specific physical constraints and design tradeoffs associated with semiconductor exciton devices.

ACKNOWLEDGMENTS

APPENDIX: FINITE-WIDTH PULSES

In order to confirm whether it is reasonable to model the pulses as infinitely short in our setting, we compare the evolution of the coherence element, $\rho_{01}(t)$, after a single DD cycle for both Gaussian and infinitely short pulses. In the presence of both the phonon coupling and finite-width pulses, no exact solution is available, however, it is possible to perturbatively include the effects of the phonons to first order in the coupling strength.[22]

Following Ref. 22, we may take advantage of the fact that the dephasing after a series of N nonoverlapping pulses, which end at $t=0$ and result in a total qubit rotation of $\pi/2$, may be written as

$$|\mathbf{P}(t)|^2 = |\mathbf{P}(t_0)|^2 \left\{ 1 - \int_0^\infty d\omega \frac{[2n_b(\omega)+1]}{\omega^2} I(\omega)|K(\omega)-e^{i\omega t}|^2 \right\},$$
(A1)

where $n_b(\omega)$ is the Bose distribution,

$$K(\omega) = \frac{1}{2i}[F(\omega)-F^*(-\omega)],$$
(A2)

$$F(\omega) = \sum_{n=1}^N \widetilde{F}_n(\omega) e^{i(\alpha_{n-1}+\omega t_n)},$$
(A3)

where t_n is the time at which the nth pulse is applied,

$$\alpha_n = \int f_n(t) dt,$$
(A4)

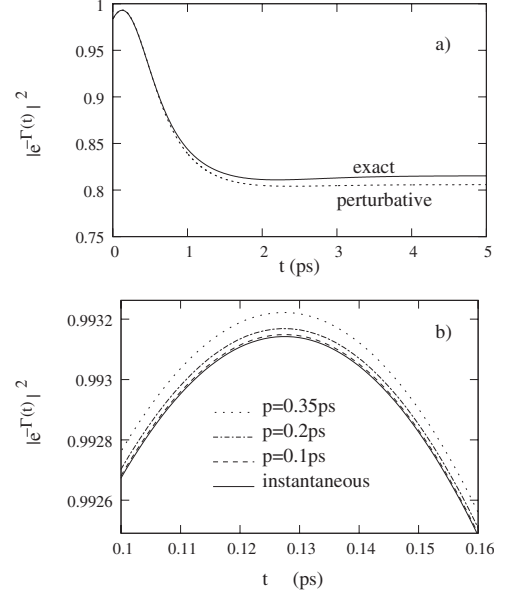where $f_n(t)$ is the profile of the nth pulse, and

FIG. 14. (a) Perturbative vs exact results for controlled decoherence in the presence of a single DD cycle consisting of instantaneous pulses. (b) Single-cycle decoherence behavior under Gaussian finite-width pulses.

$$\widetilde{F}_n(\omega) = \int e^{i\omega t} \frac{d}{dt} e^{i\widetilde{\Phi}_n} dt,$$
(A5)

$$\widetilde{\Phi}_n(t) = \int_{-\infty}^t f_n(t') dt',$$
(A6)

respectively. For illustration purposes, we choose a sequence consisting of three pulses equivalent to the first DD cycle (two bit flips) acting on a superposition state. The first pulse in the sequence occurs at $t=-2\Delta t$ and creates the state $(|0\rangle + |1\rangle)/\sqrt{2}$. Since we are interested in information storage, we assume that initialization may be achieved perfectly, that is, $f_1(t)=(\pi/2)\delta(t)$. The subsequent two pulses (the first two pulses of the DD occurring at $t=-\Delta t$ and 0) are a negative π rotation followed by a π rotation, respectively.

Figure 14(a) compares the perturbative results against the exact results both for instantaneous pulses at 4 K and $\Delta t = 0.2$ ps. For the exact results, we sample the dephasing after the sequence has been turned off using the following expression for $\Gamma(t)$, which describes the dephasing in the presence of an arbitrary sequence of N pulses:[30]

$$\Gamma(t) = \int_0^\infty d\omega \frac{2I(\omega)}{\omega^2} \coth\left(\frac{\hbar\omega}{2k_B T}\right)|y^N(\omega t)|^2,$$
(A7)

where

$$y_N(z) = 1 + (-1)^{N+1} e^{iz} + 2\sum_{m=1}^N (-1)^m e^{iz\delta_m},$$
(A8)

with the jth pulse occurring at $\delta_j t$. The two approaches are in excellent agreement especially for fraction of picosecond timescales, i.e., up to when the next DD cycle would begin.

Now that we have shown that the perturbative approach is a suitable way of modeling the dephasing, we proceed to incorporating the finite width of the pulses. We model them as Gaussian and again assume that the initial state may be created perfectly. Therefore,

$$f_1(t) = \delta(t), \tag{A9}$$

$$f_2(t) = -\frac{\sqrt{\pi}}{p}\exp\left(-\frac{t^2}{p^2}\right), \tag{A10}$$

$$f_3(t) = \frac{\sqrt{\pi}}{p}\exp\left(-\frac{t^2}{p^2}\right), \tag{A11}$$

where $2p$ is the width of the pulse. This allows for the dephasing to be calculated after the final pulse has ended according to Eq. (A1). Figure 14(b) compares the perturbative results for instantaneous pulses with those for Gaussian pulses. The curves are practically indistinguishable over the scale of Fig. 14(a). In Fig. 14(b), results are shown for the peak in the coherence following the final pulse of Fig. 14(a).

For a pulse of width $2p = \Delta t/10$, it can be seen that the dephasing is nearly identical ($\approx 0.01\%$ change) to that in the presence of infinitely short pulses. Furthermore, it can be seen that there is still only a very small change in the dephasing up to $p = 0.035$ ps, above this value, the pulses cannot be considered as nonoverlapping and the model described by Eq. (A1) fails.

Interestingly, it can be noticed that there is a slight decrease in the dephasing for Gaussian pulses compared to instantaneous pulses. This may be understood by observing that the pulse envelope enters the calculation in the form of the nonlinear spectrum $K(\omega)$, which is a functional of the pulse shape $f(t)$. The introduction of a finite-width pulse suppresses the high-frequency part of $K(\omega)$ (see Fig. 2 in Refs. 22 and 33 for related results), therefore, it reduces the integral in $|\mathbf{P}(t)|^2$ resulting in a smaller dephasing compared to delta pulses. While this transient improvement may be offset by error accumulation over long pulse trains, the above results provide strong indication that modeling the evolution with instantaneous pulses yields an adequate starting point for short-term storage purposes as investigated in text.

---

*ida500@york.ac.uk

[1] M. A. Nielsen and I. L. Chuang, *Quantum Computation and Quantum Information* (Cambridge University Press, Cambridge, England, 2000).

[2] See, e.g., Fortschr. Phys. **48**, Vol. 9–11 (2000), Special Focus Issue on Experimental Proposals for Quantum Computation, edited by S. Braunstein and H.-K. Lo.

[3] P. M. Petroff, A. Lorke, and A. Imamoglu, Phys. Today **54**(5), 46 (2001).

[4] See e.g., I. D'Amico, E. Pazy, P. Zanardi, E. Biolatti, R. C. Iotti, F. Rossi, F. Troiani, U. Hohenester, and E. Molinari, *Semiconductor Macroatoms: Basic Physics and Quantum-Device Applications* (Imperial College, London, World Scientific, Singapore, 2005).

[5] P.-C. Chen, C. Piermarocchi, and L. J. Sham, Phys. Rev. Lett. **87**, 067401 (2001); X.-Q. Li, Y. W. Wu, D. Steel, D. Gammon, T. H. Stievater, D. S. Katzer, D. Park, C. Piermarocchi, and L. J. Sham, Science **301**, 809 (2003); A. Nazir, B. W. Lovett, S. D. Barrett, T. P. Spiller, and G. A. D. Briggs, Phys. Rev. Lett. **93**, 150502 (2004); I. D'Amico, Microelectron. J. **37**, 1440 (2006); T. P. Spiller, I. D'Amico, and B. W. Lovett, New J. Phys. **9**, 20 (2007); A. Kolli, B. W. Lovett, S. C. Benjamin, and T. M. Stace, Phys. Rev. Lett. **97**, 250504 (2006); T. E. Hodgson, M. F. Bertino, N. Leventis, and I. D'Amico, J. Appl. Phys. **101**, 114319 (2007).

[6] B. Krummheuer, V. M. Axt, and T. Kuhn, Phys. Rev. B **65**, 195313 (2002).

[7] A. Vagov, V. M. Axt, and T. Kuhn, Phys. Rev. B **66**, 165312 (2002).

[8] B. Krummheuer, V. M. Axt, T. Kuhn, I. D'Amico, and F. Rossi, Phys. Rev. B **71**, 235329 (2005).

[9] A. Vagov, V. M. Axt, T. Kuhn, W. Langbein, P. Borri, and U. Woggon, Phys. Rev. B **70**, 201305 (2004).

[10] U. Haeberlen, *High Resolution NMR in Solids: Selective Averaging* (Academic, New York, 1976); C. P. Slichter, *Principles of Magnetic Resonance* (Springer-Verlag, New York, 1992).

[11] L. Viola and S. Lloyd, Phys. Rev. A **58**, 2733 (1998).

[12] L. Viola, E. Knill, and S. Lloyd, Phys. Rev. Lett. **82**, 2417 (1999).

[13] K. Khodjasteh and D. A. Lidar, Phys. Rev. Lett. **95**, 180501 (2005); Phys. Rev. A **75**, 062310 (2007).

[14] L. Viola and E. Knill, Phys. Rev. Lett. **94**, 060502 (2005); L. F. Santos and L. Viola, *ibid.* **97**, 150501 (2006).

[15] O. Kern and G. Alber, Phys. Rev. Lett. **95**, 250501 (2005).

[16] N. Shenvi, R. de Sousa, and K. B. Whaley, Phys. Rev. B **71**, 224411 (2005); R. de Sousa, N. Shenvi, and K. B. Whaley, *ibid.* **72**, 045330 (2005).

[17] W. Zhang, V. V. Dobrovitski, L. F. Santos, L. Viola, and B. N. Harmon, Phys. Rev. B **75**, 201302(R) (2007); W. Zhang, N. P. Konstantinidis, V. V. Dobrovitski, B. N. Harmon, L. F. Santos, and L. Viola, *ibid.* **77**, 125336 (2008).

[18] W. M. Witzel and S. Das Sarma, Phys. Rev. Lett. **98**, 077601 (2007); Phys. Rev. B **76**, 241303(R) (2007).

[19] W. Yao, R.-B. Liu, and L. J. Sham, Phys. Rev. B **74**, 195301 (2006).

[20] J. R. Petta, A. C. Johnson, J. Taylor, E. A. Laaird, A. Yacoby, M. D. Lukin, C. M. Marcus, M. P. Hanson, and A. C. Gossard, Science **309**, 2180 (2005).

[21] E. Fraval, M. J. Sellars, and J. J. Longdell, Phys. Rev. Lett. **95**, 030506 (2005).

[22] V. M. Axt, P. Machnikowski, and T. Kuhn, Phys. Rev. B **71**, 155305 (2005).

[23] E. Biolatti, I. D'Amico, P. Zanardi, and F. Rossi, Phys. Rev. B **65**, 075306 (2002).

[24] G. M. Palma, K.-A. Suominen, and A. K. Ekert, Proc. R. Soc. London, Ser. A **452**, 567 (1996).

[25] In our problem, the requirement $T_c \lesssim \tau_c$ may be regarded as a *necessary* condition for accurate DD. In general DD settings, a

sufficient condition is provided by convergence of the Magnus expansion approximating the evolution propagator, see Ref. 10 and, for instance, F. Casas, J. Phys. A **40**, 15001 (2007) for a recent convergence analysis.

[26] At ~300 K, second- and higher-order processes involving optical phonons would start to contribute to the system decoherence.

[27] M. Bayer, G. Ortner, O. Stern, A. Kuther, A. A. Gorbunov, A. Forchel, P. Hawrylak, S. Fafard, K. Hinzer, T. L. Reinecke, S. N. Walck, J. P. Reithmaier, F. Klopf, and F. Schäfer, Phys. Rev. B **65**, 195315 (2002).

[28] E. Pazy, E. Biolatti, T. Calarco, I. D'Amico, P. Zanardi, F. Rossi,

and P. Zoller, Europhys. Lett. **62**, 175 (2003).

[29] E. Pazy, I. D'Amico, P. Zanardi, and F. Rossi, Phys. Rev. B **64**, 195320 (2001).

[30] G. S. Uhrig, Phys. Rev. Lett. **98**, 100504 (2007); New J. Phys. **10**, 083024 (2008).

[31] B. Lee, W. M. Witzel, and S. Das Sarma, Phys. Rev. Lett. **100**, 160505 (2008); L. Cywinski, R. M. Lutchyn, C. P. Nave, and S. Das Sarma, Phys. Rev. B **77**, 174509 (2008).

[32] L. Viola and E. Knill, Phys. Rev. Lett. **90**, 037901 (2003).

[33] P. Sengupta and L. P. Pryadko, Phys. Rev. Lett. **95**, 037202 (2005).